Approach to blind image deconvolution by multiscale subband decomposition and independent component analysis

Ivica Kopriva

Department of Electrical and Computer Engineering, The George Washington University, 801 22nd Street, N.W., Washington, D.C. 20052, USA, and Division of Laser and Atomic Research and Development, Rudjer Bošković Institute, Bijenička cesta 54, P.O. Box 180, 10002, Zagreb, Croatia

Received May 30, 2006; revised October 26, 2006; accepted October 26, 2006; posted October 30, 2006 (Doc. ID 71481); published March 14, 2007

A single-frame multichannel blind image deconvolution technique has been formulated recently as a blind source separation problem solved by independent component analysis (ICA). The attractive feature of this approach is that neither origin nor size of the spatially invariant blurring kernel has to be known. To enhance the statistical independence among the hidden variables, we employ multiscale analysis implemented by wavelet packets and use mutual information to locate a subband with the least dependent components, where the basis matrix is learned by means of standard ICA. We show that the proposed algorithm is capable of performing blind deconvolution of nonstationary signals that are not independent and identically distributed processes. The image poses these properties. The algorithm is tested on experimental data and compared with state-of-the-art single-frame blind image deconvolution algorithms. Our good experimental results demonstrate the viability of the proposed concept. © 2007 Optical Society of America

OCIS codes: 070.6020, 100.1830, 100.3020, 100.3190, 100.7410.

1. INTRODUCTION

The goal of image deconvolution is to reconstruct the original image from an observation that is degraded by a spatially invariant blurring process and noise. Neglecting the noise term, the process is modeled as a convolution of a blurring kernel $h(s,t)$ with an original source image $f(x,y)$ as

$$g(x,y) = \sum_{s=-K}^{K} \sum_{t=-K}^{K} h(s,t) f(x+s, y+t), \tag{1}$$

where K denotes the support size of the blurring kernel. If the blurring kernel is known, few nonblind algorithms are available to reconstruct the original image $f(x,y)$.[1] However, it is not always possible to measure or obtain information about the blurring kernel. That is why blind deconvolution (BD) algorithms are important. They can be divided into those that estimate the blurring kernel $h(s,t)$ first and then restore the original image by some of the nonblind methods[1] and those that estimate the original image $f(x,y)$ and the blurring kernel simultaneously. To estimate the blurring kernel, a support size has to be either given or estimated. To use the appropriate parametric model of the blurring process, *a priori* knowledge about the nature of the blurring process is quite often assumed to be available.[2] It is not always possible to know the characteristics of the blurring process. Methods that estimate the blurring kernel and original image simultaneously use either statistical or deterministic priors of the original image, the blurring kernel, and the noise.[2] This leads to a computationally expensive maximum-likelihood estimation usually implemented by an expectation-maximization algorithm. In addition, exact distributions of the original image required by the maximum-likelihood algorithm are usually unknown. One of the most representative algorithms from this class is the blind Richardson–Lucy (R-L) algorithm originally derived for nonblind deconvolution of astronomical images.[3,4] It has been later formulated in Ref. 5 for BD and then modified by an iterative restoration algorithm in Ref. 6. This version of the blind R-L algorithm is implemented in MATLAB command deconvblind. It will be used in Section 3 for the comparison with the wavelet-packet (WP) subband decomposition independent component analysis (SDICA) approach. To overcome difficulties associated with the standard BD algorithms, an approach was proposed in Ref. 7 based on quasi-maximum likelihood with an approximate of the probability density function. It, however, assumed that the original image has sparse or super-Gaussian distribution. This is generally not true because image distributions are mostly sub-Gaussian. To overcome that difficulty, applying a sparsifying transform to a blurred image was proposed in Ref. 7. However, the design of such a transform requires knowledge of at least the typical class of images to which the original image belongs. In that case, training data can be used to design the sparsifying transform.

Multivariate data analysis methods, such as independent component analysis[8,9] (ICA), might be used to solve the BD problem as a blind source separation (BSS) problem, where the unknown blurring process is absorbed into a mixing matrix. The advantage of the ICA approach would be that no *a priori* knowledge about the origin and size of the support of the blurring kernel is required. However, the multichannel image required by ICA is not always available. Even if it is, it would require the blurring kernel to be nonstationary, which is true for the blur caused by atmospheric turbulence,[10] but it is not true for the out-of-focus blurred images, for example. Therefore, an approach to single-frame multichannel blind deconvolution that requires minimum *a priori* information about the blurring process and original image would be of great interest.

A single-frame multichannel representation was proposed in Ref. 11. It was based on a bank of 2D Gabor filters[12] because of their ability to realize multichannel filtering. ICA algorithms have been applied in Ref. 11 to a multichannel image in order to extract the source image and two spatial derivatives along the x and y directions. However, there is a critical condition that the source image and their spatial derivatives must be statistically independent. In general, this is not true, as already observed in Ref. 13. Consequently, the quality of the image restoration by the proposed single-frame multichannel approach depends on how well each particular image satisfies the statistical independence assumption. Therefore, an extension of the ICA approach formulated in Ref. 11 is given in Refs. 14–16. In those papers, it has been shown that single-frame multichannel BD can be formulated as a nonnegative matrix factorization (NMF) problem with sparseness constraints imposed on the unknown mixing vector or source image.

We present here the multiscale SDICA approach to blind image deconvolution. It follows ideas of the recently formulated algorithms[17–21] for separation of statistically dependent signals. One approach to solve such a problem, and to relax the statistical independence assumption, is to assume that the wideband source signals are dependent, but there exist some narrow subbands where they are independent. This assumption leads to SDICA. We refer interested readers to Refs. 17–21 for specific details related to SDICA implementations. In this paper, we implement SDICA by multiscale decomposition using WPs[22] because of their computationally efficient implementation through an iterative filter bank. The subband with the least dependent subcomponents is detected by measuring the mutual information between corresponding nodes in the wavelet trees. We use the computationally efficient small cumulant-based approximation of mutual information. Owing to the fact that the WP is a linear transform, the unknown basis or mixing matrix is obtained by the standard ICA algorithm executed on the selected subband. The source image is recovered by applying the inverse of the obtained basis matrix to the original multichannel representation of the observed (degraded) image. The advantage of this approach to BD with respect to the recently introduced NMF approach is that potential problems associated with the nonuniqueness of the matrix decomposition and selection of sparseness constraints are avoided. Once the subband with least dependent components is detected, standard and well-understood ICA algorithms can be used to learn the basis matrix.

The rest of the paper is organized as follows. We describe in Section 2 the multiscale SDICA approach to blind image deconvolution. A comparative experimental performance evaluation is given in Section 3 for sparse and nonsparse images degraded by the out-of-focus blur. The multiscale SDICA BD algorithm is compared with the blind single-frame R–L algorithm,[5,6] the single-frame multichannel ICA BD algorithm,[11] and the single-frame multichannel NMF algorithm.[14–16] The most significant conclusions are given in Section 4.

2. MULTISCALE SDICA BLIND IMAGE DECONVOLUTION

Before proceeding to describe the multiscale SDICA BD algorithm, we shall rewrite the image observation model given by Eq. (1) in the lexicographical notation

$$\mathbf{g} = \mathbf{H}\mathbf{f}, \tag{2}$$

assuming an image dimensionality of $M \times N$ pixels, where $\mathbf{g}, \mathbf{f} \in R_{0+}^{MN}$, $\mathbf{H} \in R_{0+}^{MN\times MN}$. The observed image vector $\mathbf{g}$ and the original image vector $\mathbf{f}$ are obtained from their 2D counterparts by the row-stacking procedure. Equation (2) can be rewritten as

$$\begin{pmatrix} \mathbf{g}_0 \\ \mathbf{g}_1 \\ \mathbf{g}_2 \\ \cdots \\ \mathbf{g}_{M-1} \end{pmatrix} = \begin{bmatrix} \mathbf{H}_0 & \mathbf{H}_{-1} & \mathbf{H}_{-2} & \mathbf{0} \\ \mathbf{H}_1 & \mathbf{H}_0 & \mathbf{H}_{-1} & \\ \mathbf{H}_2 & \mathbf{H}_1 & \mathbf{H}_0 & \\ \hline \mathbf{0} & & \cdots & \mathbf{H}_0 \end{bmatrix} \begin{pmatrix} \mathbf{f}_0 \\ \mathbf{f}_1 \\ \mathbf{f}_2 \\ \cdots \\ \mathbf{f}_{M-1} \end{pmatrix},$$

$$= \begin{bmatrix} h_{j,0} & h_{j,-1} & h_{j,-2} & 0 \\ h_{j,1} & h_{j,0} & h_{j,-1} & \\ h_{j,2} & h_{j,1} & h_{j,0}\cdots & \\ \hline 0 & & & \cdots h_{j,0} \end{bmatrix}. \tag{3}$$

The matrix $\mathbf{H}$ is a block-Toeplitz matrix.[23] It absorbs into itself the blurring kernel $h(s,t)$, assuming that at least the size of it, K, is known. In Eqs. (3), vectors $\mathbf{g}_j$ and $\mathbf{f}_j$ represent jth rows of the corresponding 2D images. The block-Toeplitz structure of $\mathbf{H}$ can be further approximated by a block-circular structure:

$$\mathbf{H} \cong \begin{bmatrix} \mathbf{H}_0 & \mathbf{H}_{-1} & \mathbf{H}_{-2} & \mathbf{H}_1 \\ \mathbf{H}_1 & \mathbf{H}_0 & \mathbf{H}_{-1} & \\ \mathbf{H}_2 & \mathbf{H}_1 & \mathbf{H}_0 & \\ \hline \mathbf{H}_{-1} & & & \cdots\mathbf{H}_0 \end{bmatrix},$$

$$\mathbf{H}_j = \begin{bmatrix} h_{j,0} & h_{j,-1} & h_{j,-2} & h_{j,1} \\ h_{j,1} & h_{j,0} & h_{j,-1} & \\ h_{j,2} & h_{j,1} & h_{j,0}\cdots & \\ \hline h_{j,-1} & & & \cdots h_{j,0} \end{bmatrix}. \tag{4}$$

This approximation introduces small degradations at the image boundaries, but it enables expression of Eq. (2) by circular convolution. This is crucially important for frequency-domain implementations of deblurring algorithms. We present here an updated equation of the blind R-L algorithm.[5,6] It will be used in Section 3 for comparison purposes. While in Ref. 5, Eqs. (4) and (5), the R-L algorithm is implemented in the spatial domain on the component level, we give the equivalent block implementation in the frequency domain:

$$\hat{\mathbf{H}}_{i+1}^{(k)} = [(\hat{\mathbf{f}}^{(k-1)})^T(\mathbf{g} \oslash (\hat{\mathbf{H}}_i^k \hat{\mathbf{f}}^{(k-1)}))]\hat{\mathbf{H}}_i^{(k)},$$

$$\hat{\mathbf{f}}_{i+1}^{(k)} = [\hat{\mathbf{f}}_i^{(k)} \otimes (\mathbf{H}^{(k)T}(\mathbf{g} \oslash (\mathbf{H}^{(k)}\hat{\mathbf{f}}_i^{(k)})))]. \quad (5)$$

The symbol $\otimes$ denotes componentwise multiplication, and the symbol $\oslash$ denotes componentwise division. The index i is used to denote internal iteration of the blind R-L algorithm, while k denotes the main iteration index. Multiplicative update rules automatically ensure positivity of both the blurring kernel and the reconstructed image. A rescaled version of the blind R-L algorithm, which converges faster, is obtained by the minimization of the generalized Kullback–Leibler divergence (also called I divergence).[24] We see from Eqs. (5) the problem with the blind R-L algorithm. Although the blurring kernel incorporated in the block-circulant matrix $\mathbf{H}$ is estimated from the observed image, the support size K must be either known or estimated. This difficulty can be resolved by multivariate data analysis methods, such as ICA.[8,9] Here, the BD problem is treated as a BSS problem, where the unknown blurring process is absorbed into a mixing matrix. An approach has been proposed in Ref. 11 to obtain a multichannel version of the observed image $\mathbf{g}$, which is required by ICA. It was based on a bank of 2D Gabor filters,[12] which were used because of their ability to realize multichannel filtering. The Gabor filters have the following real and imaginary parts, respectively,

$$R(x,y) = G(x,y)\cos\left(\frac{\pi}{\sigma}\varphi(x,y)\right),$$

$$I(x,y) = G(x,y)\sin\left(\frac{\pi}{\sigma}\varphi(x,y)\right), \quad (6)$$

where

$$G(x,y) = \exp\left(-\frac{x^2+y^2}{2\sigma^2}\right),$$

$$\varphi(x,y) = x\cos\left(\frac{\pi}{Q}q\right) + y\sin\left(\frac{\pi}{Q}q\right), \quad q = 0,1,\ldots,Q-1.$$

The parameter q regulates one of the Q spatial orientations. The parameter $\sigma = \sqrt{2^\omega}$, with $\omega = 1,2,\ldots\,\Omega$, regulates one of the Ω spatial frequencies. The 2D Gabor filters used in this paper are shown in Fig. 1 with $\Omega = 2$ and $Q = 4$. The first two rows show real and imaginary parts of 2D Gabor filters for $\omega = 1$, and the last two rows show them for $\omega = 2$. Each column shows one of the four orientations. Real and imaginary parts of the Gabor filters are used as separate filters. The key insight in Ref. 11 was that the original image $f(x+s,y+t)$ can be approximated by a Taylor-series expansion around $f(x,y)$, giving

$$f(x+s,y+t) = f(x,y) + sf_x(x,y) + tf_y(x,y) + s^2 f_{xx}(x,y) + t^2 f_{yy}(x,y) + \cdots . \quad (7)$$

This enables one to rewrite Eq. (1) as

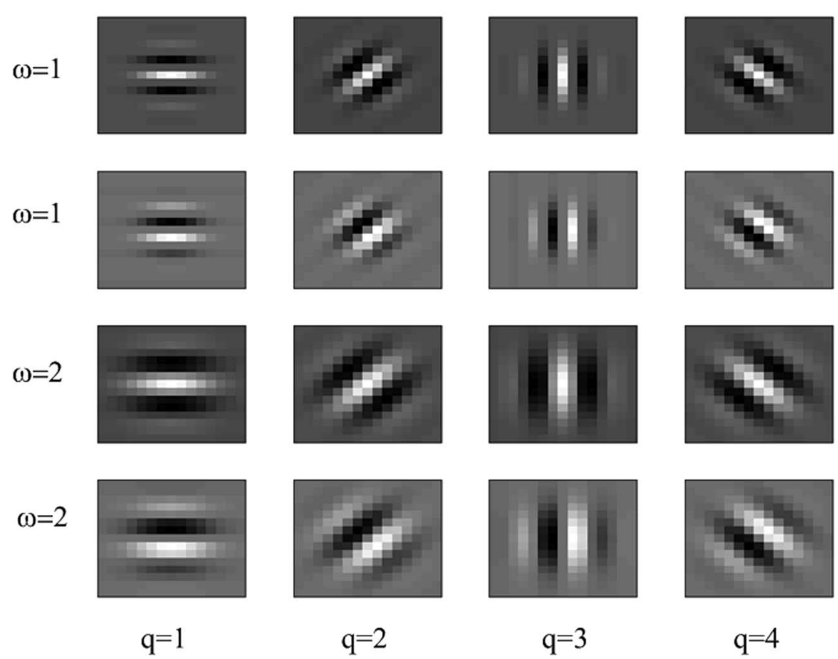

Fig. 1. Gabor filters for two spatial frequencies, $\Omega = 2$, and four orientations, $Q = 4$. The first two rows show real and imaginary parts of 2D Gabor filters for $\omega = 1$, and the last two rows show them for $\omega = 2$. Each column shows one of the four orientations.

$$g_1(x,y) = a_{11}f(x,y) + a_{12}f_x(x,y) + a_{13}f_y(x,y) + a_{14}f_{xx}(x,y) + a_{15}f_{yy}(x,y) + \cdots , \quad (8)$$

where $a_{11}=\Sigma_{s=-K}^{K}\Sigma_{t=-K}^{K}h(s,t)$, $a_{12}=\Sigma_{s=-K}^{K}\Sigma_{t=-K}^{K}sh(s,t)$, $a_{13}=\Sigma_{s=-K}^{K}\Sigma_{t=-K}^{K}th(s,t)$, $a_{14}=\Sigma_{s=-K}^{K}\Sigma_{t=-K}^{K}s^2h(s,t)$, and $a_{15}=\Sigma_{s=-K}^{K}\Sigma_{t=-K}^{K}t^2h(s,t)$. To have a clear notation, we have indexed the degraded image $g(x,y)$ in Eq. (8). f_x and f_y represent first-order spatial derivatives in the x and y directions, while f_{xx} and f_{yy} represent second-order spatial derivatives. When Gabor filters are applied to a blurred image, a new set of observed images is obtained:

$$g_{l+1}(x,y) = a_{(l+1)1}f(x,y) + a_{(l+1)2}f_x(x,y) + a_{(l+1)3}f_y(x,y) + a_{(l+1)4}f_{xx}(x,y) + a_{(l+1)5}f_{yy}(x,y) + \cdots , \quad (9)$$

where $a_{(l+1)1}=\Sigma_{s=-K'}^{K'}\Sigma_{t=-K'}^{K'}h_l'(s,t)$, $a_{(l+1)2}=\Sigma_{s=-K'}^{K'}\Sigma_{t=-K'}^{K'}sh_l'(s,t)$, $a_{(l+1)3}=\Sigma_{s=-K'}^{K'}\Sigma_{t=-K'}^{K'}th_l'(s,t)$, $a_{(l+1)4}=\Sigma_{s=-K'}^{K'}\Sigma_{t=-K'}^{K'}s^2h_l'(s,t)$, and $a_{(l+1)5}=\Sigma_{s=-K'}^{K'}\Sigma_{t=-K'}^{K'}t^2h_l'(s,t)$. $h_l'(s,t)$ represents convolution of the appropriate lth Gabor filter with $h(s,t)$, $K'=K+J-1$, and J represents the order of the Gabor filter. This leads to multichannel representation:

$$\mathbf{G} = \begin{pmatrix} \mathbf{g}_1^T \\ \mathbf{g}_2^T \\ \cdots \\ \mathbf{g}_{L+1}^T \end{pmatrix} \cong \begin{bmatrix} a_{11} & a_{12} & a_{13} & a_{14} & a_{15} & \cdots \\ a_{21} & a_{22} & a_{23} & a_{24} & a_{25} & \cdots \\ \hdashline a_{(L+1)1} & a_{(L+1)2} & a_{(L+1)3} & a_{(L+1)4} & a_{(L+1)5} & \cdots \end{bmatrix} \times \begin{pmatrix} \mathbf{f}^T \\ \mathbf{f}_\mathbf{x}^T \\ \mathbf{f}_\mathbf{y}^T \\ \mathbf{f}_\mathbf{xx}^T \\ \mathbf{f}_\mathbf{yy}^T \\ \cdots \end{pmatrix} = \mathbf{AF}, \quad (10)$$

where $\mathbf{G}\in R_{0+}^{(L+1)\times MN}$, $\mathbf{A}\in R_{0+}^{(L+1)\times P}$, $\mathbf{F}\in R_{0+}^{P\times MN}$. P represents the number of the sources that ought to be estimated.

We present here results and conditions necessary for the stochastic differentiability of the random source signal $\mathbf{f}$.[25] Their importance is in establishing conditions for the existence of the Taylor-series expansion [Eq. (7)] and the linear mixture model (LMM) expression (10)]. We assume that $\mathbf{f}$ has been obtained from its 2D counterpart by the Peano–Hillbert space-filling curve,[26] which is mapping that preserves neighborhood statistics. First, we present two important results that relate (nonstationarity) stationarity and linear signal representation. If the signal $\mathbf{f}$ is stationary, it can be represented by the linear space-invariant generative model:

$$f(p) = \sum_{r=0}^{R} b(r)\epsilon(p-r), \quad (11)$$

where ϵ represents an independent and identically distributed (i.i.d.) driving signal. The moving-average generative model of the order R can be replaced by the equivalent autoregressive or autoregressive moving-average model with the order significantly less than R. If the signal $\mathbf{f}$ is nonstationary, the linear signal model becomes space variant:

$$f(p) = \sum_{r=0}^{R} b(p,r)\epsilon(p-r). \quad (12)$$

We comment here that image $\mathbf{f}$ is a nonstationary signal because its statistics vary locally; i.e., $pdf(f(p_1)) \neq pdf(f(p_2))$ when p_1 and p_2 differ significantly. It means that for the image the first-order stationarity requirement does not hold.[25] We also comment that image $\mathbf{f}$ is a process with colored statistics; i.e., it is not an i.i.d. process. This is consequence of the known phenomenon that neighborhood pixels are usually highly correlated. Consequently, its autocorrelation function $\rho_\mathbf{f}(\tau)$ differs from the delta function.

First-order spatial derivative $\dot{\mathbf{f}}$ of the stationary signal $\mathbf{f}$ is defined if the first-order derivative of the autocorrelation function at the lag zero is zero; i.e., $\dot{\rho}_\mathbf{f}(0)=0$. We point out that this condition is not fulfilled for an i.i.d. process, the autocorrelation function of which is a delta function. Therefore, the Taylor-series expansion [Eq. (7)] for such a signal does not exist. Consequently, the LMM model [expression (10)] also does not exist. Thus, i.i.d. signals cannot be blindly deconvolved by the proposed algorithm. Because the image is not an i.i.d. process, it is not affected by this finding. If the source image $\mathbf{f}$ is a stationary process with colored statistics, it can also not be deconvolved by the proposed algorithm. The stationary signal can be represented by a linear space-invariant generative signal model [Eq. (11)]. Assuming that $\mathbf{b}$ represents the impulse response of the linear space-invariant signal generative model, it is impossible to distinguish the blurring filter $\mathbf{h}$ from the linear convolution of the blurring filter and modeling filter: $\mathbf{h}*\mathbf{b}$. Thus, the proposed algorithm will deconvolve the i.i.d. driving sequence ϵ. When the signal is stationary with colored statistics, the algorithm will have the whitening effect. The presented analysis implies that signals amenable for BD by the proposed approach must be nonstationary and non-i.i.d. processes. The image has these properties. Thus, in regard to blind image deconvolution we only have to prove existence of the Taylor-series expansion [Eq. (7)] for the nonstationary non- i.i.d. process. In Refs. 25 and 27 are derived conditions for stochastic differentiability for stationary signals only. Provided that space-varying filter $\mathbf{b}$ is stationary with respect to the independent variable p, we can use the linear generative model of the nonstationary signal [Eq. (12)] to define derivatives of the nonstationary signal. In such a case we define

$$\dot{f}(p) \cong \sum_{r=0}^{R} \frac{\mathrm{d}b(p,r)}{\mathrm{d}p}\epsilon(p-r). \quad (13)$$

We can proceed with the higher-order derivatives if the stochastic differentiability conditions for stationary signal $\mathbf{b}$ are fulfilled.[25,27] Therefore, for nonstationary signals, Taylor-series expansion [Eq. (7)] and the LMM [expression (10)] exist. However, we cannot make a conclusion regarding statistical independence between a signal and its stochastic derivatives as is the case for the stationary signal.[25] Thus, it is justified to use some of the methods derived for enhancing statistical independence between the hidden variables in the LMM [expression (10)]. In this paper we propose an SDICA algorithm to solve this problem.

The ICA algorithms can be applied to expression (10) to extract the source image **f**. We emphasize that the main role of the Gabor filters in the LMM [expression (10)] is to provide $L+1$ linearly independent measurements. The other property of Gabor filters, to decompose input image into sparse images, is not of crucial importance in the WP SDICA approach to BD as it was in the NMF approach with sparseness constraints.[14–16] In this respect, the WP SDICA approach is more robust with respect to the order of Gabor filters. After initial testing, we set the order to $J=7$. Regarding the higher-order terms in expansions (7)–(9), it is evident that the order will influence the quality of the approximation of the degraded image. The higher-order terms can be dropped from the expansion if the size of the blurring kernel, K, is small or the source image has negligible higher-order spatial derivatives. This implies that a first-order approximation would be valid only for a weak degradation process. In contrast, the case with strong degradation and large K will require the higher-order terms in the expansions (7) and (9). The number of terms in the expansions is equivalent to the number of unknown sources, P, in the BSS context. Because we know neither the strength of the degradation nor the character of the source image in advance, this number ought to be estimated. The standard procedure is to inspect singular values of the sample data covariance matrix $\hat{\mathbf{R}}_{\mathbf{GG}}$, where the hat sign denotes the sample estimate.[9] Alternatively, more sophisticated methods for the estimation of the number of sources, such as Akaike's information criterion or minimum description length criterion, may be also used.[9] The ijth entry of $\hat{\mathbf{R}}_{\mathbf{GG}}$ is obtained as

$$[\hat{\mathbf{R}}_{\mathbf{GG}}]_{ij} = \frac{1}{MN}\sum_{m=1}^{MN} \mathbf{g}_i(m)\mathbf{g}_j(m), \qquad i,j \in \{1,2,\ldots,L+1\}.$$

The estimate of the number of sources, $\hat{P}$, is obtained from the singular values of $\hat{\mathbf{R}}_{\mathbf{GG}}$ as

$$\hat{P} = \max_{p}\left(\frac{\sum_{t=1}^{p}\sigma_t^2}{\sum_{t=1}^{L+1}\sigma_t^2} < \epsilon\right),$$

where ϵ is some predefined threshold close to 1. We point out that a greater number of sources will not influence performance of the WP SDICA algorithm as long as $P \leq L+1$. It will affect performance of the NMF algorithm more significantly. This is due to the known property of the NMF methods that the number of sensors, $L+1$, is to be several times greater than the number of sources P. Thus, we expect that the WP SDICA algorithm would perform better than NMF algorithms in the conditions of the strong degradation.

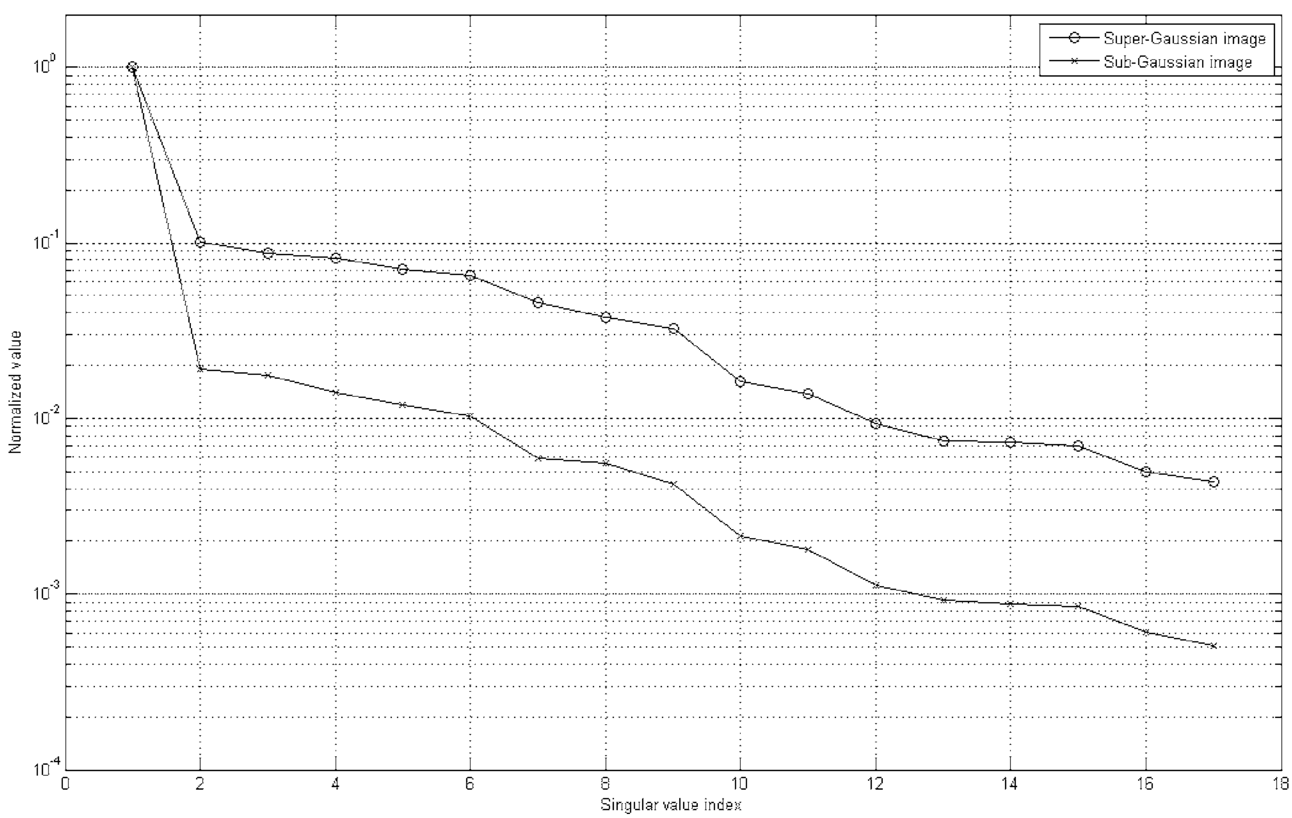

Fig. 2. Normalized singular values of the sample data covariance matrices of the multichannel images: crosses, defocused sub-Gaussian image shown in Fig. 3; circles, defocused super-Gaussian image shown in Fig. 9.

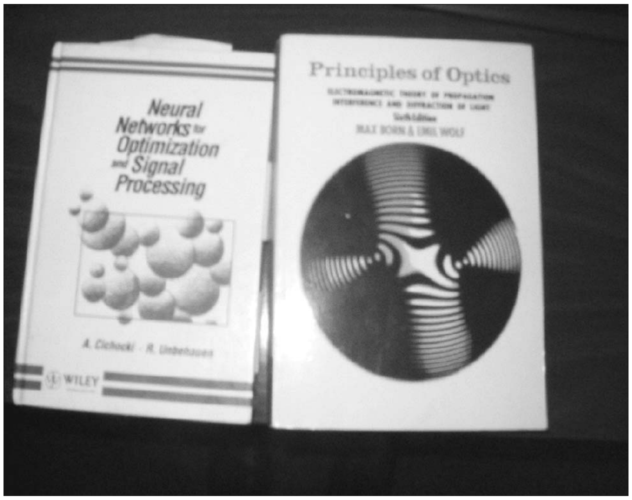

Fig. 3. Nonsparse (sub-Gaussian) image degraded by out-of-focus blur obtained by a digital camera in manually defocused mode.

We show in Fig. 2 singular values of the sample data covariance matrices obtained from the multichannel versions, expression (10), for a defocused sub-Gaussian image (Fig. 3) and a defocused super-Gaussian image (Fig. 9 below). In the case of the sub-Gaussian image, the first three singular values contributed 92% of the overall energy (sum of all singular values). In the case of the super-Gaussian image, the first three singular values contribute 71.4%, and the first five contribute 83% of the overall energy. This indicates that the defocusing degradation in the experimental images was weak. Regarding other types of the degradation, it has been demonstrated in Ref. 16 that the NMF algorithm with sparseness constraints was successful in deblurring an image degraded by weak atmospheric turbulence. The same linear multichannel model given by expression (10) was used in that experiment. There is no reason that WP SDICA will not work for some other type of degradation, such as atmospheric turbulence.

We emphasize that no *a priori* information about the blurring kernel is assumed so far. There is, however, a critical condition for the source images that must hold in order for ICA algorithms to work. Images $\mathbf{f}$, $\mathbf{f_x}$, $\mathbf{f_y}$, $\mathbf{f_{xx}}$, and $\mathbf{f_{yy}}$ must be statistically independent. This is, in general, not true as first observed in Ref. 13 and later in Refs. 14–16. To use the ICA algorithm to solve the BD problem of expression (10) as a BSS problem, we assume that the wideband source signals $\mathbf{f}$, $\mathbf{f_x}$, $\mathbf{f_y}$, $\mathbf{f_{xx}}$, and $\mathbf{f_{yy}}$ are dependent, but there exist some narrow subbands where they are less dependent. This is an assumption that has been proven very successful in solving the BSS problem for statistically dependent sources.[17–21] It has been introduced on the basis of empirical evidence, which shows that multichannel signals usually have the concentration of statistical dependence much higher in the low-frequency part of the spectrum than in the high-frequency part of it. This empirical evidence can be easily verified if an innovations filter is found from the multichannel model [expression (10)]. The innovations have the property of being more statistically independent than the original process as well as being more non-Gaussian. Because of that property, they were proposed in Ref. 28 as a method to increase the accuracy of the standard ICA algorithms. The innovations filter, also known as the prediction-error filter, is found from the multichannel model by means of Levinson's algorithm.[29] The filter is adapted to the local statistical conditions and has higher attenuation in the parts of the spectrum where statistical dependence is higher.

An adaptive subband decomposition scheme, such as produced by WP, should be successful in finding the subband with the least dependent components. We use the linearity property of the WP to transform data model [expression (10)] into

$$\mathrm{WP}(\mathbf{G}) = \mathbf{A}\mathrm{WP}(\mathbf{F}). \tag{14}$$

This property was exploited extensively in the various versions of the sparse ICA. It has been found that either the WP or the short-time Fourier transform is very useful for obtaining a new representation of data, which is sparser than the original formulation. As has been shown, executing ICA in the sparse domain produced more accurate solutions for solving the linear instantaneous BSS problem. It also enabled the solution of an underdetermined (more sources than sensors) BSS problem.[30–34] In the particular case of the WP, we express each source image in terms of its decomposition coefficients:

$$\mathbf{f}^{j}_{kn}(\xi) = \sum_{l} c^{j}_{knl}\varphi_{jl}(\xi), \tag{15}$$

where j represents the scale level, k represents the subband index, n represents the source index, and l represents the shift index. $\varphi_k(\xi)$ is the chosen wavelet, also called the atom or element of the representation space, and c^{j}_{kml} are decomposition coefficients. In our implementation of the described WP SDICA algorithm, we have used shift-invariant 2D WP decomposition. Regarding the type of the wavelet, we have also used symmlets[22] with eight vanishing moments. In accordance with the linear image observation model of expression (10), the source image $\mathbf{f}_n$ in Eq. (15) belongs to the set $\{\mathbf{f}, \mathbf{f_x}, \mathbf{f_y}, \mathbf{f_{xx}}, \mathbf{f_{yy}}, \ldots\}$. The multichannel observed image $\mathbf{G}$ is expressed in the source image representation space as

$$\mathbf{g}^{j}_{kn}(\xi) = \sum_{l} y^{j}_{knl}\varphi_{jl}(\xi). \tag{16}$$

Let vectors $\mathbf{y}_l$ and $\mathbf{c}_l$ be constructed from the lth coefficients of the mixtures and sources, respectively. From expressions (10) and (15), and using the orthogonality property of the functions $\varphi_j(\xi)$, we obtain

$$\mathbf{y}_l = \mathbf{A}\mathbf{c}_l. \tag{17}$$

If additive noise is present, this relation holds approximately. From expressions (10) and (17), we see the same relation between signals in the original domain and the WP representation domain. Inserting Eq. (17) into expression (10) and using Eq. (15), we obtain

$$\mathbf{G}^{j}_{k}(\xi) = \mathbf{A}\mathbf{F}^{j}_{k}(\xi), \tag{18}$$

as introduced by Eq. (14). For each component $\mathbf{g}_n$ of the multichannel observed image $\mathbf{G}$, the WP transform will create a tree with nodes that correspond to the subbands at the appropriate scale. To select the subband with least dependent components $\mathbf{f}_n$, we measure the mutual information between the corresponding nodes in the wavelet trees. For this purpose, we use the small cumulant approximation of the Kullback–Leibler divergence. It represents an exact measure of the mutual information, and its approximation is obtained under weak correlation and weak non-Gaussianity assumptions[35]:

$$\begin{aligned}\hat{I}_c^j(\mathbf{g}_1^j,\mathbf{g}_2^j,\ldots,\mathbf{g}_{L+1}^j) \approx & \frac{1}{4}\sum_{\substack{1\leq k<l\leq L+1\\ k\neq l}} \mathrm{cum}^2(\mathbf{g}_k^j,\mathbf{g}_l^j)\\ &+\frac{1}{24}\sum_{\substack{1\leq k<l\leq L+1\\ k\neq l}} (\mathrm{cum}^2(\mathbf{g}_k^j,\mathbf{g}_k^j,\mathbf{g}_l^j)\\ &+\mathrm{cum}^2(\mathbf{g}_k^j,\mathbf{g}_l^j,\mathbf{g}_l^j))\\ &+\frac{1}{48}\sum_{\substack{1\leq k<l\leq L+1\\ k\neq l}} (\mathrm{cum}^2(\mathbf{g}_k^j,\mathbf{g}_k^j,\mathbf{g}_k^j,\mathbf{g}_l^j)\\ &+\mathrm{cum}^2(\mathbf{g}_k^j,\mathbf{g}_k^j,\mathbf{g}_l^j,\mathbf{g}_l^j)\\ &+\mathrm{cum}^2(\mathbf{g}_k^j,\mathbf{g}_l^j,\mathbf{g}_l^j,\mathbf{g}_l^j)).\end{aligned} \tag{19}$$

In Eq. (19), cum( ) denotes second-, third-, and fourth-order cross cumulants.[36,37] The approximation of the joint mutual information as the sum of pairwise mutual information is commonly used in the ICA community to simplify computational complexity of the linear instantaneous ICA algorithms.[38] Once the subband with the least dependent components is selected, we obtain either an estimation of the inverse of the basis matrix $\hat{\mathbf{W}}$ or an estimation of the basis matrix $\hat{\mathbf{A}}$ by applying standard ICA algorithms to the model of Eq. (18). Reconstructed source images $\hat{\mathbf{F}}$, however, are obtained by applying $\hat{\mathbf{W}}$ to the original multichannel image $\mathbf{G}$:

$$\hat{\mathbf{F}} = \hat{\mathbf{W}}\mathbf{G}. \tag{20}$$

We summarize the multiscale SDICA blind image deconvolution approach in the following five steps:

1. Obtain the multichannel version $\mathbf{G}$ of degraded image $\mathbf{g}$ by applying the 2D Gabor filter bank, expressions (6)–(10).
2. Perform multiscale WP decomposition of each component of the multichannel image $\mathbf{G}$. A wavelet tree will be associated with each component of $\mathbf{G}$, Eqs. (14)–(17).
3. Select the subband with the least dependent components by estimating mutual information between corresponding nodes (subbands) in the wavelet trees, expressions (18) and (19).
4. Estimate the basis matrix $\hat{\mathbf{A}}$ or its inverse $\hat{\mathbf{W}}$ by executing the standard ICA algorithm for the linear static problem on the selected subband, Eq. (18).
5. Obtain the deconvolved image by applying $\hat{\mathbf{W}}$ to multichannel image $\mathbf{G}$, Eq. (20).

3. EXPERIMENTAL RESULTS

We present in this section BD results for sub-Gaussian and super-Gaussian images experimentally degraded by the out-of-focus blur. The images have been acquired by a digital camera in a manually defocused mode. We have compared the multiscale SDICA blind image deconvolution algorithm with the blind R-L algorithm, single-frame multichannel ICA blind image deconvolution algorithm, and single-frame multichannel NMF algorithm.

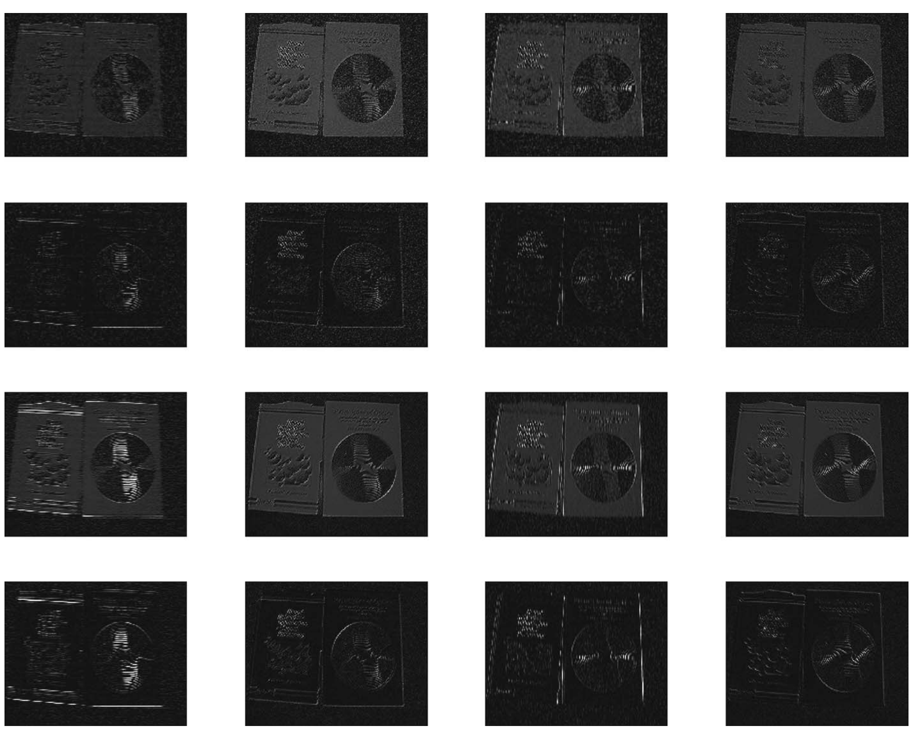

Fig. 4. Multichannel version of the degraded image shown in Fig. 3, produced by the 2D Gabor filter bank shown in Fig. 1.

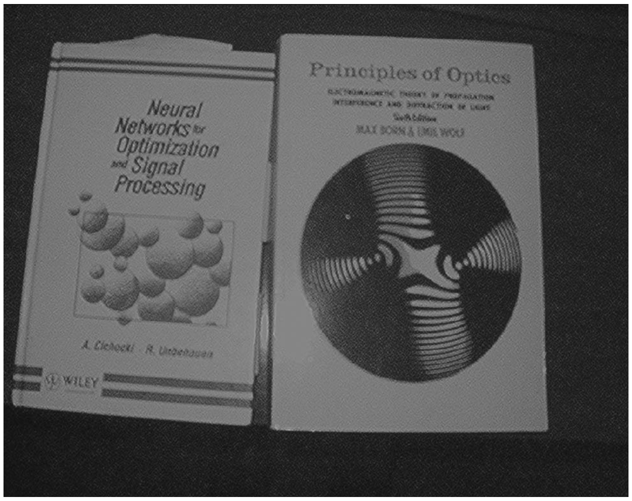

Fig. 5. Nonsparse image reconstructed with the multiscale SDICA algorithm.

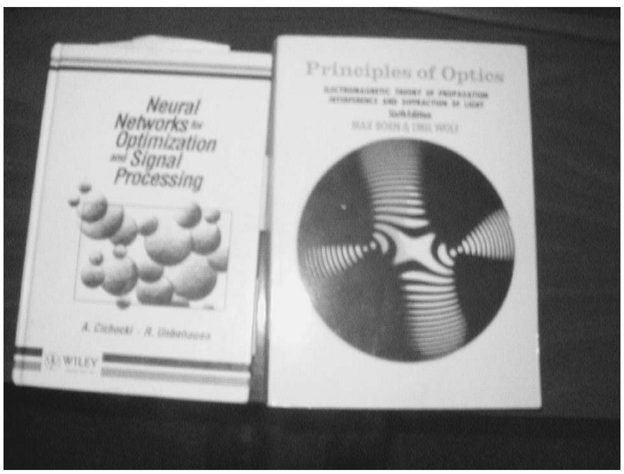

Fig. 6. Nonsparse (sub-Gaussian) image reconstructed by direct application of the JADE algorithm to the linear multichannel model [expression (10)].

We show in Fig. 2 normalized singular values of the sample data covariance matrices $\hat{\mathbf{R}}_{\mathbf{GG}}$. The covariance matrices were estimated from the multichannel representation, expression (10), of the sub-Gaussian defocused image shown in Fig. 3 and super-Gaussian defocused image shown in Fig. 9 (next page) Kurtosis of the sub-Gaussian image is −1.76, while kurtosis of the super-Gaussian image is 7.68. In the case of the sub-Gaussian image, the first three singular values contribute 92% of the overall energy. Therefore, in the blind image deconvolution of the sub-Gaussian image in Fig. 3, by means of the linear multichannel model of expression (10) and the WP SDICA algorithm, we have selected the number of sources $P=3$. In the case of the super-Gaussian image in Fig. 9 the first singular value that corresponds to the source image is well distinguished while the next four singular values have similar values. This would suggest that the number of sources in the linear multichannel model of expression (10) is $P=5$; i.e., second-order terms in the expansions in expressions (4)–(6) exist. The first five singular values contribute 83% of the overall energy. We note that, although results reported for the super-Gaussian image were obtained for $P=5$ sources, we have also tried reconstruction with $P=3$ sources. There was no visible difference between the two restored images.

We show in Fig. 3 the blurred sub-Gaussian image obtained by a digital camera in a manually defocused mode. The multichannel version of the same image produced by the 2D Gabor filter bank is shown in Fig. 4. Figure 5 shows the image reconstructed by the multiscale SDICA algorithm, while Fig. 6 shows the image reconstructed by the single-frame multichannel ICA algorithm.[11] The JADE algorithm[39] has been used to perform ICA. The image restored by the single-frame multichannel ICA algorithm has poor quality due to already noted assumptions made about the statistical independence between the source image and its spatial derivatives. The JADE algorithm has also been used to find the inverse of the basis matrix at the subband selected by the multiscale SDICA algorithm. The best subband has been found at the scale level 2. Due to the computational complexity of the 2D wavelet tree, the number of nodes grows as 4^j, with j being the scale level. Hence, we did not proceed with decomposition at level 3 or higher. There is, however, experience from experiments with 1D signals, which shows that improvement in separation quality at higher decomposition levels is not comparable with the increase of computational costs.

Figure 7 shows the image restored by the blind R-L algorithm after five iterations with a circular blurring kernel and radius of $R=3$ pixels. Because the blurred image of Fig. 3 was not highly defocused, the blind R-L algorithm with the kernel size of $R=3$ pixels produced good results. But they were still inferior to the result produced by the multiscale SDICA algorithm shown in Fig. 5. We comment that the blind R-L algorithm had to be run several times for different values of the size of the blurring kernel R. Then the image with the best quality was chosen. There are no such problems with the multiscale SDICA algorithm. For the sake of completeness, we show in Fig. 8 the image deconvolved by single-frame multi-

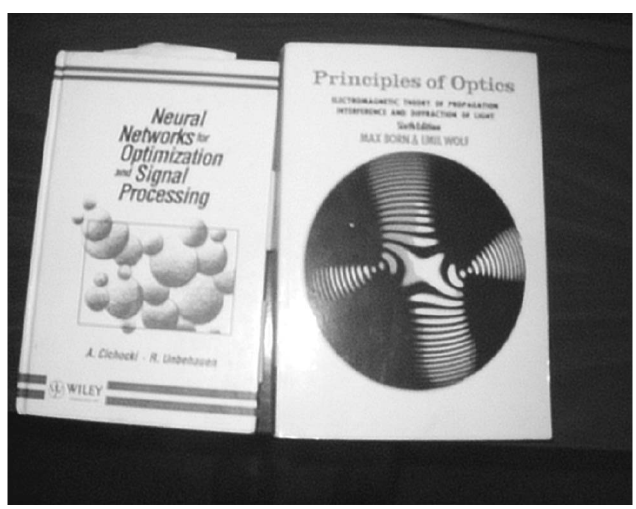

Fig. 7. Nonsparse image reconstructed by the blind Richardson–Lucy algorithm after five iterations with a circular blurring kernel with radius of $R=3$ pixels.

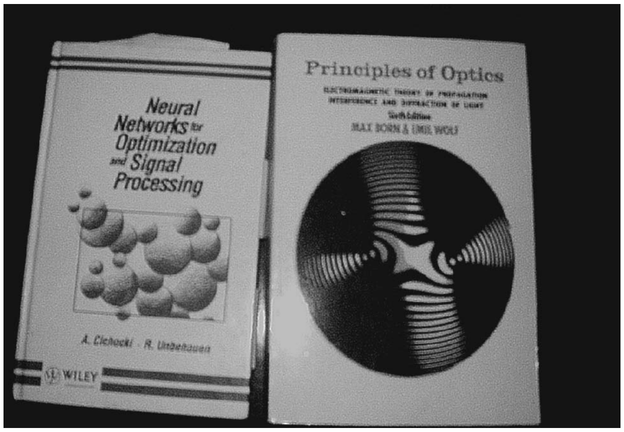

Fig. 8. Nonsparse image reconstructed with the single-frame multichannel NMF algorithm.

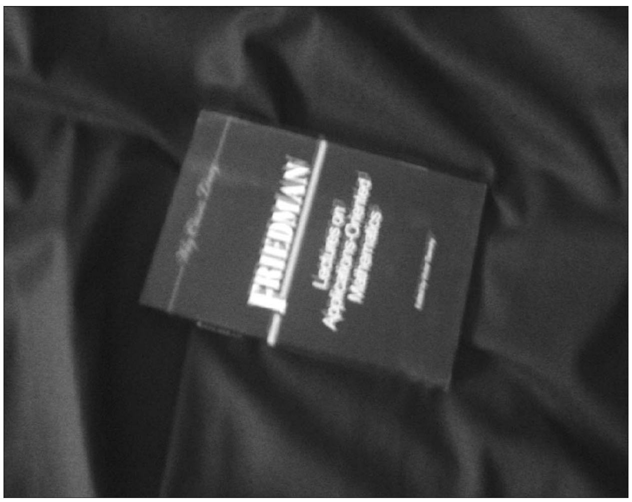

Fig. 9. Sparse (super-Gaussian) image degraded by out-of-focus blur obtained by a digital camera in manually defocused mode. Image was acquired under low-light-level conditions.

channel NMF algorithms.[14–16] This image is of comparable quality with the image obtained by the multiscale SDICA algorithm, except that the paradigm used to formulate BD was completely different. The advantage of the multiscale SDICA approach in relation to the NMF approach with sparseness constraints is that problems with the nonuniqueness of the factorization and selections of constraints are avoided. Once the subband with least dependent components is selected, well-understood algorithms for solving linear instantaneous BSS problems[8,9] are used to learn either the basis matrix or its inverse. Also, if the inspection of the singular values indicates that a greater number of sources ought to be used in the linear multichannel model, the NMF algorithms would require a greater order of the multichannel model to retain the same level of the restoration quality. We note that the images shown in Fig. 3 and 6–8 have already been shown in Refs. 14–16. Some important references to NMF with constraints are Refs. 40–42.

To illustrate performance of the described multiscale SDICA algorithm for the blurred super-Gaussian images, we have recorded the blurred image by a digital camera in the manually defocused mode under low-light-level conditions. It is shown in Fig. 9. Figure 10 is the image reconstructed by the multiscale SDICA algorithm. The image was restored under conditions already described for Fig. 5. Figure 11 shows the image reconstructed by the single-frame multichannel ICA algorithm,[11] where the JADE algorithm[39] was used again to execute an ICA. Again, the image restored by the single-frame multichannel ICA algorithm has poor quality due to the assumptions made about the statistical independence between the source image and its spatial derivatives. Figure 12 shows the image restored by the blind R-L algorithm after five iterations with a circular blurring kernel and radius of $R=3$ pixels. Because the blurred image in Fig. 9 was not highly defocused, the blind R-L algorithm with the kernel size of $R=3$ pixels produced a good result but still inferior to that produced by the multiscale SDICA algorithm shown in Fig. 10. Again, we comment that the blind R-L algorithm had to be run several times for different values of the size of the blurring kernel R. Then the image with the best quality could be chosen. There are no such problems with the multiscale SDICA algorithm. For the sake of completeness, we show in Fig. 13 the image deconvolved by single-frame multichannel NMF algorithms.[14–16] This im-

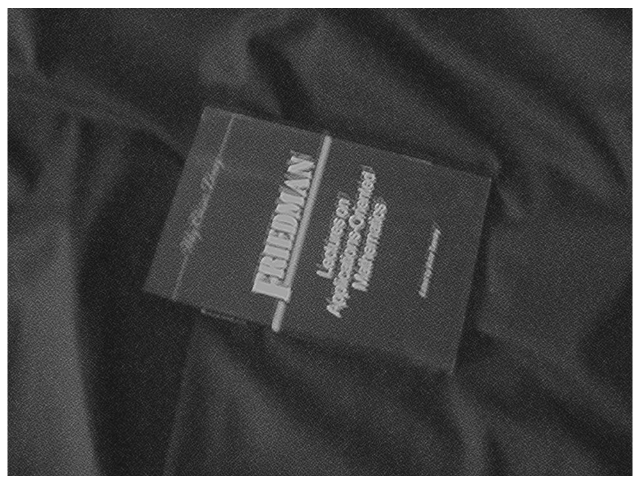

Fig. 10. Sparse image reconstructed with the multiscale SDICA algorithm.

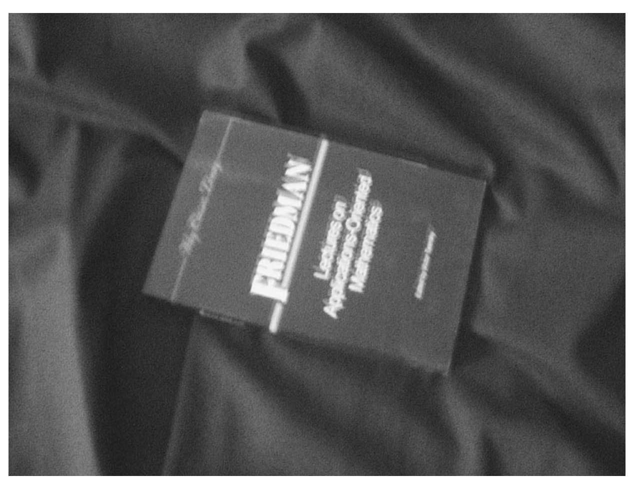

Fig. 11. Sparse (super-Gaussian) image reconstructed by direct application of the JADE algorithm to the linear multichannel model [expression (10)].

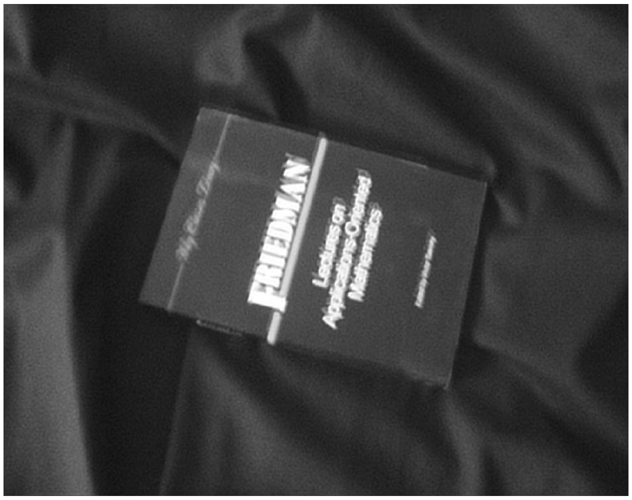

Fig. 12. Sparse image reconstructed by the blind Richardson–Lucy algorithm after five iterations with a circular blurring kernel with radius of $R=3$ pixels.

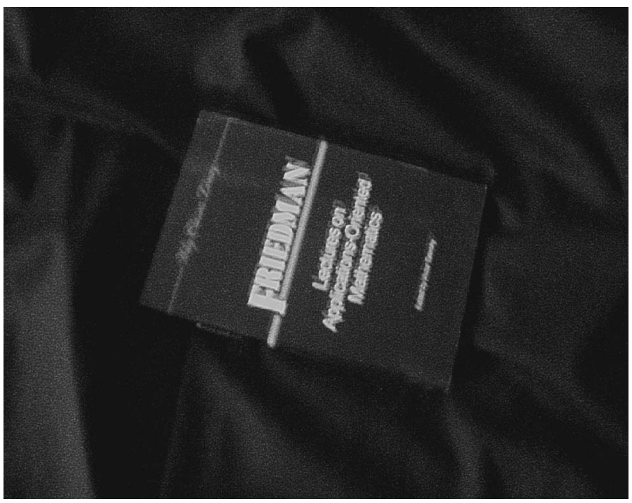

Fig. 13. Sparse image reconstructed with the single-frame multichannel NMF algorithm.

age is of comparable quality with the image obtained by the multiscale SDICA algorithm except that the paradigm used to formulate BD was completely different and has potential problems avoided by the procedure introduced in this paper. We note again that images shown in Figs. 9 and 11–13 have already been shown in Ref. 16.

4. CONCLUSION

A multiscale subband decomposition independent component analysis approach to blind image deconvolution has been derived. By relating statistical properties of the image to the existence of the linear mixture model, we show that the proposed algorithm is capable of performing blind deconvolution of nonstationary and non-i.i.d. processes. The image has these properties. In relation to most blind image deconvolution algorithms, this approach does not require information about the size of the blurring kernel or the statistics of the unknown source image. Thus, the algorithm is completely unsupervised. This makes it attractive for applications in astronomy, medical imaging, microscopy, night vision, and other imaging modalities. Good experimental results with defocused sub-Gaussian and super-Gaussian images confirmed the viability of the proposed approach to blind image deconvolution.

ACKNOWLEDGMENTS

The author thanks the reviewers for their constructive comments. David Nagel's help in proofreading the manuscript is also gratefully acknowledged.

The author can be reached by e-mail at ikopriva@gmail.com.

REFERENCES

1. M. R. Banham and A. K. Katsaggelos, "Digital image restoration," IEEE Signal Process. Mag. **14**, 24–41 (1997).
2. D. Kundur and D. Hatzinakos, "Blind image deconvolution," IEEE Signal Process. Mag. **13**, 43–64 (1996).
3. W. H. Richardson, "Bayesian-based iterative method of image restoration," J. Opt. Soc. Am. **62**, 55–59 (1972).
4. L. B. Lucy, "An iterative technique for rectification of observed distribution," Astron. J. **79**, 745–754 (1974).
5. D. A. Fish, A. M. Brinicombe, E. R. Pike, and J. G. Walker, "Blind deconvolution by means of the Richardson–Lucy algorithm," J. Opt. Soc. Am. A **12**, 58–65 (1995).
6. D. S. C. Biggs and M. Andrews, "Acceleration of iterative image restoration algorithms," Appl. Opt. **36**, 1766–1775 (1997).
7. M. M. Bronstein, A. Bronstein, M. Zibulevsky, and Y. Y. Zeevi, "Blind deconvolution of images using optimal sparse representations," IEEE Trans. Image Process. **14**, 726–736 (2005).
8. A. Hyvärinen, J. Karhunen, and E. Oja, *Independent Component Analysis* (Wiley Interscience, 2001).
9. A. Cichocki and S. Amari, *Adaptive Blind Signal and Image Processing* (Wiley, 2002).
10. I. Kopriva, Q. Du, H. Szu, and W. Wasylkiwskyj, "Independent component analysis approach to image sharpening in the presence of atmospheric turbulence," Opt. Commun. **233**, 7–14 (2004).
11. S. Umeyama, "Blind deconvolution of blurred images by use of ICA," Electron. Commun. Jpn. Part III: Fund. Electron. Sci. **84**, 1–9 (2001).
12. J. G. Daugman, "Complete discrete 2-D Gabor transforms by neural networks for image analysis and compression," IEEE Trans. Acoust., Speech, Signal Process. **36**, 1169–1179 (1988).
13. M. Numata and N. Hamada, "Image restoration of multichannel blurred images by independent component analysis," in *Proceedings of 2004 RISP International Workshop on Nonlinear Circuit and Signal Processing*, Hawaii, March 5–7, 2004, pp. 197–200.
14. I. Kopriva, "Single-frame multichannel blind deconvolution by nonnegative matrix factorization with sparseness constraints," Opt. Lett. **30**, 3135–3137 (2005).
15. I. Kopriva and D. Nuzillard, "Non-negative matrix factorization approach to blind image deconvolution," Lect. Notes Comput. Sci. **3889**, 966–973 (2006).
16. I. Kopriva, D. J. Garrood, and V. Borjanović, "Single frame blind image deconvolution by non-negative sparse matrix factorization," Opt. Commun. **266**, 456–464 (2006).
17. A. Cichocki, "Blind source separation: new tools for extraction of source signals and denoising," in *Independent Component Analyses, Wavelets, Unsupervised Smart Sensors, and Neural Networks III*, H. Szu, ed., Proc. SPIE **5818**, 11–25 (2005).
18. A. Cichocki and P. Georgiev, "Blind source separation

algorithms with matrix constraints," IEICE Trans. Fundamentals **E86-A**, 522–531 (2003).
19. T. Tanaka and A. Cichocki, "Subband decomposition independent component analysis and new performance criteria," in *Proceedings of the IEEE Conference on Acoustics, Speech, and Signal Processing* (IEEE, 2004), pp. 541–544.
20. K. Zhang and L. W. Chan, "An adaptive method for subband decomposition ICA," Neural Comput. **18**, 191–223 (2006).
21. K. Zhang and L. W. Chan, "Enhancement of source independence for blind source separation," Lect. Notes Comput. Sci. **3889**, 731–738 (2006).
22. M. V. Wickerhauser, *Adapted Wavelet Analysis from Theory to Software* (Peters, 1994).
23. R. L. Lagendijk and J. Biemond, *Iterative Identification and Restoration of Images* (Kluwer Academic, 1991).
24. C. L. Bryne, "Accelerating the EMML algorithm and related iterative algorithms by rescaled block-iterative methods," IEEE Trans. Image Process. **7**, 100–109 (1998).
25. M. B. Priestley, *Spectral Analysis and Time Series* (Academic, 1981).
26. W. M. Lam and J. M. Shapiro, "A class of fast algorithms for the Peano–Hillbert space filling curve," in *Proceedings of the IEEE International Conference Image Processing (ICIP-94)* (IEEE, 1994), Vol. 1, pp. 638–641.
27. A. M. Yaglom, *Introduction to the Theory of Stationary Random Functions* (Prentice Hall, 1962).
28. A. Hyvärinen, "Independent component analysis for time-dependent stochastic processes," in *Proceedings of the International Conference on Artificial Neural Networks* (Springer-Verlag Telos, 1998), pp. 541–546.
29. S. J. Orfanidis, *Optimum Signal Processing: An Introduction*, 2nd ed. (Macmillan, 1988).
30. M. Zibulevsky, P. Kisilev, Y. Zeevi, and B. Pearlmutter, "Blind source separation via multinode sparse representation," in *Advances in Neural Information Processing Systems* (Morgan Kaufman, 2002), pp. 185–191.
31. Y. Li, A. Cichocki, and S. Amari, "Analysis of sparse representation and blind source separation," Neural Comput. **16**, 1193–1234 (2004).
32. P. Georgiev, F. Theis, and A. Cichocki, "Sparse component analysis and blind source separation of underdetermined mixtures," IEEE Trans. Neural Netw. **16**, 992–996 (2005).
33. Y. Li, S. Amari, A. Cichocki, D. W. C. Ho, and S. Xie, "Underdetermined blind source separation based on sparse representation," IEEE Trans. Signal Process. **54**, 423–437 (2006).
34. P. Kisilev, M. Zibulevsky, and Y. Y. Zeevi, "Multiscale framework for blind separation of linearly mixed signals," J. Mach. Learn. Res. **4**, 1339–1363 (2003).
35. J. F. Cardoso, "Dependence, correlation and Gaussianity in independent component analysis," J. Mach. Learn. Res. **4**, 1177–1203 (2003).
36. D. R. Brillinger, *Time Series Data Analysis and Theory* (McGraw-Hill, 1981).
37. P. McCullagh, *Tensor Methods in Statistics* (Chapman & Hall, 1995).
38. P. Comon, "Independent component analysis, a new concept?" Signal Process. **36**, 287–314 (1994).
39. J. F. Cardoso and A. Souloumiac, "Blind beamforming for non-Gaussian signals," IEE Proc. F, Radar Signal Process. **140**, 362–370 (1993).
40. P. O. Hoyer, "Non-negative matrix factorization with sparseness constraints," J. Mach. Learn. Res. **5**, 1457–1469 (2004).
41. D. D. Lee and H. S. Seung, "Learning the parts of objects by non-negative matrix factorization," Nature **401**, 788–791 (1999).
42. A. Cichocki, R. Zdunek, and S. Amari, "Csiszár's divergences for non-negative matrix factorization: family of new algorithms," Lect. Notes Comput. Sci. **3889**, 32–39 (2006).